Towards customized heat treatments and mechanical properties in the LPBF-processed Ti-6Al-2Sn-4Zr-6Mo alloy

Alessandro Carrozza *, Alberta Aversa, Paolo Fino, Mariangela Lombardi

Department of Applied Science and Technology, Politecnico Di Torino, Corso Duca degli Abruzzi 24, 10129 Torino, Italy

HIGHLIGHTS

- The LPBF process induces the formation of softening α" orthorhombic martensite in the Ti-6Al-2Sn-4Zr-6Mo alloy.
- Distinct transformations occur at different annealing temperatures: α" decomposition, residual stress relaxation and β complete recrystallization.
- Post-processing heat treatments can be specifically tailored to tune the final microstructure/mechanical properties of the material.
- Optimal combinations of strength and ductility can be achieved.

GRAPHICAL ABSTRACT
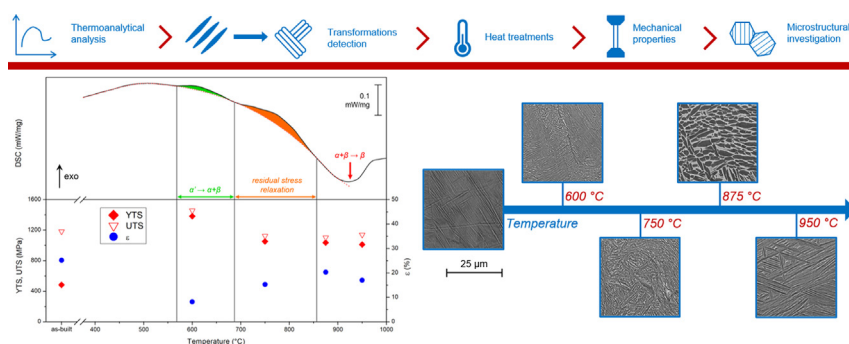
ABSTRACT

The Ti-6Al-2Sn-4Zr-6Mo alloy was recently successfully processed using the laser powder bed fusion technology. This material is characterized by a very low strength in the as-built state, due to the presence of α" martensite. In this work, the transformations taking place at different temperatures in this alloy were investigated with the aim of achieving the necessary knowledge to customize the mechanical properties via heat treatments. Martensite decomposition, residual stress relaxation and the β-transus temperature were identified at progressively increasing temperatures. Then, different annealing treatments, corresponding to the temperatures identified, were conducted. For each condition, dissimilar α + β microstructures were obtained, varying in terms of morphology (lamellar, bi-lamellar) and size of the α laths (0.5–2.2 μm). The corresponding tensile properties were also significantly different. In particular, outstanding strength values were achieved when the residual stress was retained. For higher temperatures, a slight drop in strength was coupled with an outstanding improvement in terms of ductility. Overall, the most balanced combination of tensile properties was obtained for an annealing temperature of 875 °C. In this condition, the bi-lamellar microstructure grants a reduction in the slip length due to the presence of secondary α laths.

1. Introduction

Titanium alloys are fundamental materials in certain industrial fields, such as aerospace, biomedical and automotive. The importance of these alloys is due to an ideal combination of specific properties, for instance a high strength to weight ratio, excellent

* Corresponding author.
E-mail addresses: alessandro.carrozza@polito.it (A. Carrozza), alberta.aversa@polito.it (A. Aversa), paolo.fino@polito.it (P. Fino), mariangela.lombardi@polito.it (M. Lombardi).

corrosion resistance and biocompatibility. Titanium alloys can be categorized according to their composition. In fact, the most common alloying elements can be stabilizers of the hexagonal close-packed (HCP) α phase, or the body centred cubic (BCC) β phase. The most common type of titanium alloys used in the industry is α + β, or duplex. These are characterized by the compresence of both phases at room temperature. Among these materials, the Ti-6Al-4V alloy is widely established as the most adopted solution in the industry. Instead, Ti-6Al-2Sn-4Zr-6Mo is a more β-stabilized duplex alloy that finds its usage in some niche applications, mostly in the aerospace sector (e.g. compressor disks, blades). Its adoption is mostly due to its superior creep resistance and ability to retain good mechanical properties at higher temperatures with respect to the Ti-6Al-4V alloy, whose operational temperature limit lies around 350 °C. Thus, the Ti-6Al-2Sn-4Zr-6Mo is commonly utilized for hot sections of gas turbines [1–3].

The typical industrial fields that already adopt the Ti-6Al-2Sn-4Zr-6Mo alloy revolve around high-quality/complex components, manufactured in small and possibly highly customizable lots. This is the ideal framework for the application of additive manufacturing (AM) technologies. Therefore, the use of these techniques to process the Ti-6Al-2Sn-4Zr-6Mo alloy is industrially promising and potentially economically advantageous. Among the AM technologies, Laser Powder Bed Fusion (LPBF) proved its reliability for titanium alloys processing. In fact, multiple Ti alloys successfully processed by means of LPBF can be found in the literature: Ti-6Al-4V [4–6], commercial purity titanium (cp-Ti) [7], Ti-24Nb-4Zr-8Sn [8], Ti-6Al-7Nb [9], Ti-21Nb-17Zr [10] and Ti-13Nb-13Zr [11]. Just recently, the Ti-6Al-2Sn-4Zr-6Mo alloy was successfully processed by LPBF for the first time [12], thus generating a certain interest on this subject in the literature [13]. In a previous work from the authors [12], the behaviour of this material, its microstructural features and mechanical properties were assessed. Certainly, the most notable feature of the Ti-6Al-2Sn-4Zr-6Mo alloy is the formation of the orthorhombic martensite α" upon rapid cooling, due to the effect of the laser. This metastable phase has a strong softening character, unlike the hexagonal α' martensite that forms in the Ti-6Al-4V alloy, which results in a severe ductility reduction and a moderate strengthening effect. The massive presence of α" results in significantly low yield strength values (≈ 500 MPa), unacceptable for most structural applications. However, as in Ti-6Al-4V, martensite decomposition can be achieved with a simple annealing heat treatment. In fact, promising tensile properties were achieved via a post-processing stress-relieving heat treatment at 750 °C, followed by furnace cooling. However, the temperature was depicted by evaluating the difference in terms of β-transus temperatures (T_β) between the Ti-6Al-2Sn-4Zr-6Mo and Ti-6Al-4V alloys. After this heat treatment, the Ti-6Al-2Sn-4Zr-6Mo alloy became superior, in terms of tensile properties, with respect to the conventional LPBF-processed Ti-6Al-4V alloy, that underwent a similar heat treatment. Nevertheless, a deep understanding on how the post-processing heat treatments affect the microstructure and mechanical properties of the LPBF-produced Ti-6Al-2Sn-4Zr-6Mo alloy is still lacking. Achieving this knowledge is fundamental for the industrial applicability of the Ti-6Al-2Sn-4Zr-6Mo alloy and to design specific post-processing routes, thus material properties, according to the final application of the component. In fact, the typical heat treatments performed on titanium parts are usually derived from years of literature and experience on conventional thermo-mechanical processing [14]. However, the LPBF technology grants microstructural features otherwise conventionally unachievable (e.g. columnar prior-β grains, local anisotropy). This is mostly due to the out-of-equilibrium conditions typically achieved during the process, which generally result in the insurgence of significant residual stresses and metastable phases (martensite). Therefore, the development of specific and innovative heat treatments, tailored on the unique microstructures obtained, appears necessary. However, to achieve that, the phase transformations occurring at different temperatures must be understood. A common way to establish the phase transformations that take place at different temperatures in a material is the differential scanning calorimetry (DSC) analysis. This methodology was already successfully adopted by several authors working on different materials [15–17]. Among these, Sallica-Leva et al. [18] adopted this technique to investigate the microstructural evolution of a LPBF-produced Ti-6Al-4 V alloy. In their work, the authors detected two separate phenomena to occur at T < T_β: residual stress relaxation and α' decomposition.

An investigation on the phase and microstructural evolutions of the LPBF-produced Ti-6Al-2Sn-4Zr-6Mo alloy is currently missing in the literature, according to the authors' knowledge. Therefore, the aim of this work was to conduct a thermoanalytical analysis to extrapolate different temperatures to be adopted for post-processing annealing treatments. Then, the microstructure and mechanical properties of the specimens were assessed to understand the influence of every phenomenon occurring. The final goal was to grant the ability to generate useful knowledge to be able to tailor post-processing routes according to the final application of a component (e.g. strength maximization, minimum ductility requirements, etc.).

2. Materials and methods

A pre-alloyed Ti-6Al-2Sn-4Zr-6Mo spherical powder supplied by TLS Technik GmbH was used as feedstock material. Further details on the powder are available elsewhere [12].

15x15x15 mm cubes and cylinders with a height of 100 mm and a diameter of 12.5 mm (horizontally built) were fabricated using an EOS M270 Dual Mode LPBF machine. The process parameters adopted are summarized in Table 1.

At first, the transformations occurring in an as-built sample at different temperatures were investigated by conducting a DSC analysis, using a Setaram TGA 92 16.18 Thermal analyser. The experiment was conducted using a heating and cooling rate of 5 °C/min and considering a maximum temperature of 1000 °C. After the first run, a second one was considered to evaluate possible differences between the thermograms.

The other samples were then heat treated according to the transformation temperatures indicated by the DSC analysis, as will be discussed in the next section of this work. All the heat treatments were carried out using a Pro.Ba VF8000/S high-vacuum furnace. In order to resemble the conditions of the DSC analyses, a heating rate of 5 °C/min was adopted and a slow cooling rate varying between 1 and 5 °C/min was achieved. All the heat treatments considered were isothermal holdings followed by furnace cooling. The different temperatures considered, and the relative denomination of the specimens are summarized in Table 2. The samples

Table 1
LPBF process parameters used to produce the specimens.

Power (W)	Scanning speed (mm/s)	Hatching distance (mm)	Platform temperature (°C)	Layer thickness (μm)	Scanning strategy
190	1100	0.1	100	30	Standard 67° EOS strategy

Table 2
Heat treatments considered in this work.

Condition	Temperature (°C)	Time (h)
HT600	600	2
HT750	750	2
HT875	875	2
HT950	950	2

were kept at the set temperatures for 2 h to provide the complete occurrence of the diffusive phenomena and their identification. In fact, this duration is quite long, as annealing treatments on titanium alloys usually last 0.5–2 h [19,20]. The temperature–time trends are instead visible in Fig. 1 and compared with the T_β range, obtained from the literature.

The cubic samples were then sectioned along the building direction, mounted and polished using silicon carbide papers with progressively finer grid. The final polishing step was performed on a synthetic cloth paper using a water-based solution of colloidal SiO_2 and oxygen peroxide. Microstructural observations were carried on after chemically etching the polished surfaces using a Kroll solution (93% H_2O, 5% HNO_3, 2% HF). A Phenom-XL scanning electron microscope (SEM) and a Tescan S9000G field emission scanning electron microscope (FESEM) were used for general imaging of the samples. The measurements of the microstructural features (width of the α laths) were assessed in terms of image analysis using the software ImageJ to perform the measurements on more than 20 high-magnification SEM micrographs per condition. Phase composition and lattice parameters determination were investigated by means of X-ray diffraction (XRD) using a PANalytical X-Pert Philips diffractometer in a Bragg Brentano configuration, operated at 40 kV and 40 mA with a Cu K_α radiation. The step size and 2θ range were 0.013° and 30-70°, respectively. The analysis of the diffraction peaks allowed to determine the lattice parameters of the phases detected. This type of analysis was already successfully adopted in a previous work from the authors in which further details on the methodology are available [24].

Vickers microhardness tests were conducted using a Leica VMHT hardness tester set to apply a load of 300 g per 15 s. The mean hardness was determined by studying 25 indentations per condition.

The cylinders in all the conditions considered were mechanically machined to obtain cylindrical tensile specimens, in compliance with ASTM E8 [25]. These specimens were characterized by a gage length of 16 mm and a 4 mm diameter. Tensile tests were performed using a Zwick Roell Z050 tensile tester set to work at a stain rate of 0.0008 s^{-1}. The yield tensile strength (YTS), ultimate tensile strength (UTS) and elongation (ε) were assessed for all the specimens investigated.

3. Results and discussion

The aim of the DSC experiment was to investigate the phenomena that occur when heating an LPBF-produced Ti-6Al-2Sn-4Zr-6Mo sample (Fig. 2). The curve relative to the as-built sample (run 1) provided two clear exothermal peaks. The first one (I), ranging from 567 to 686 °C, presented a relative maximum around 600 °C. Instead, the second one (II), covering a temperature gap between 686 and 855 °C, peaked at approximately 780 °C. A third (III) endothermic transformation that peaked at 924 °C was also detected. The experiment was conducted again on the same sample (run 2). The aim of this repetition was to evaluate whether the phenomena detected during the first run persisted after a complete recrystallization of the microstructure occurred. In fact, the temperature reached up to 1000 °C during the test, which is safely higher than the T_β values reported in the literature, ranging from 900 to 940 °C [21–23]. The exothermic peaks were completely absent in the second run, suggesting their correlation with transformations occurring exclusively in the as-built state. In a work from Sallica-Leva et al. [18], comparable exothermic features in the DSC thermogram were found, ranging from 440 to 590 °C and 760 to 850 °C, respectively. The authors attributed the former peak to residual stress relaxation phenomena and the latter to martensite (α') decomposition. However, this analysis was con-
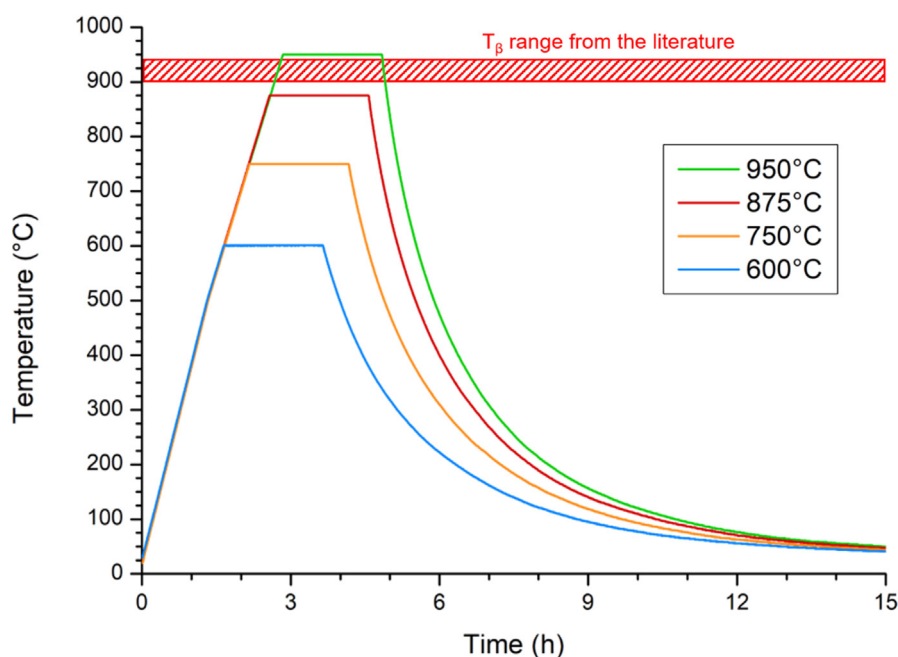

Fig. 1. Temperature-time trends for all the heat treatments considered in this work. The dashed red area represents the range in which T_β lies, as reported in different works in the literature [21–23]. (For interpretation of the references to colour in this figure legend, the reader is referred to the web version of this article.)
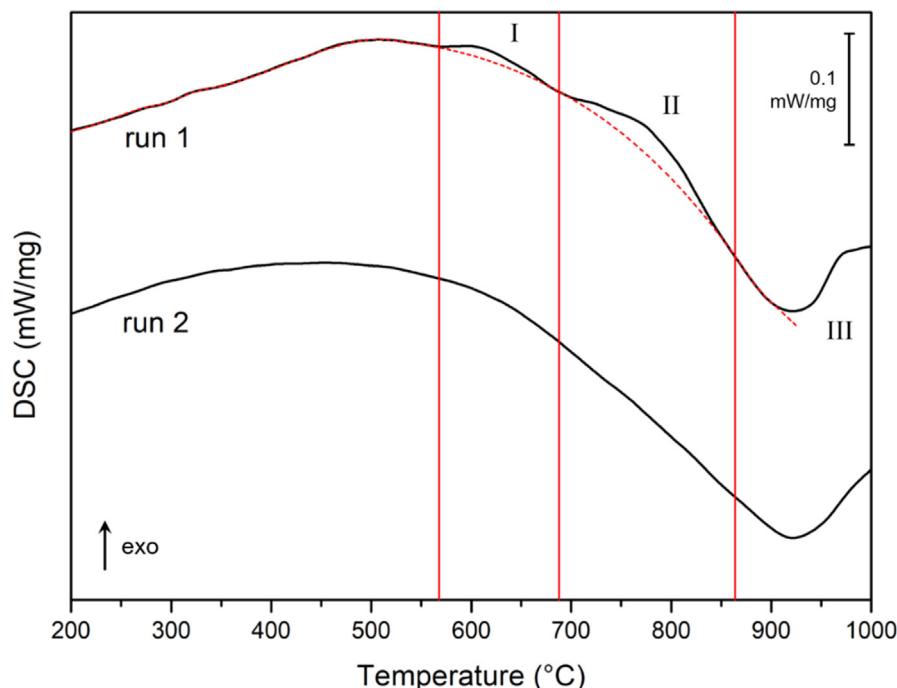
Fig. 2. DSC curves of the LPBF-processed Ti-6Al-2Sn-4Zr-6Mo alloy in the as-built state (run 1) and after recrystallization at T > T_β (run 2). The dashed red line (baseline of run 1) highlights the exothermic peaks. (For interpretation of the references to colour in this figure legend, the reader is referred to the web version of this article.)

ducted on LPBF-produced Ti-6Al-4 V samples, and a certain degree of variability is expected between the two materials, even if these shares being α + β titanium alloys. The endothermic peak III was correlated to the α + β → β transformation, hence its temperature corresponded to the T_β, which was determined to be 924.6 ± 1.1 °C. This value was calculated as the minimum of the curve, in compliance with the methodology adopted by other authors in the literature [16,26,27].

In order to further investigate the phenomena occurring during the heating ramp, a series of annealing heat treatments was performed on different cubic samples. The holding temperatures were chosen to fall within the ranges of the exothermic peaks detected in the DSC thermograph: 600 °C and 750 °C for peaks I and II, respectively. Concerning peak III, a sub-beta and a super-beta transus annealing treatments were investigated. The relative temperatures were set slightly above and below T_β, as commonly performed for duplex titanium alloys [28]. Hence, the specimens were isothermally held at 875 and 950 °C, respectively. The proximity of these temperatures to T_β was aimed at: creating a high amount of metastable β phase, in the 875 °C case, and preventing excessive grain growth at 950 °C, due to the significantly higher self-diffusion coefficient of titanium in the β phase [29]. The microstructures relative to all the conditions considered are reported in Fig. 3.

In the as-built state, the typical microstructural features of LPBF-produced duplex titanium alloys were detected: columnar prior-β grains grown parallel to the building direction, visible melt-pools and martensitic needles (Fig. 3a). As already stated in a previous work [12], the Ti-6Al-2Sn-4Zr-6Mo alloy forms orthorhombic α" martensite, instead of the conventional hexagonal α' martensite, typically generated in more α-stabilized duplex alloys (e.g. Ti-6Al-4 V). Upon annealing at 600 °C (Fig. 3b), no traces of residual α" were found. Instead, an α + β microstructure was detected, in which α lamellae were enveloped by a thin β layer. The α laths mostly shared the same crystallographic orientations, thus lamellar colonies were clearly visible. Moreover, thick α layers were found in correspondence of the prior-β grain boundaries (α_GB). This

microstructural change suggested that peak I in the DSC thermogram (Fig. 2) corresponded to the α" → α + β diffusion-driven transformation (martensite decomposition). In the HT750 sample (Fig. 3c), the duplex α + β microstructure persisted. However, a lower degree of order was found in the α laths, as in fact the colonies disappeared in favour of multiple orientations of the lamellae. This outcome can be generally correlated to two different phenomena: a variation in the cooling rate or phases (α, β) partitioning during the heat treatment [30]. As visible in Fig. 1, the cooling rates achieved in all the conditions were comparable at high temperatures. Therefore, the variation in the α laths arrangement was the result of the different α and β equilibrium amounts during the isothermal holding, which is a function of the temperature itself. In fact, the nucleation of new α laths takes place in correspondence of high-temperature β phase during cooling. Furthermore, some larger α laths, characterized by a significantly lower aspect ratio, were found in the HT750 specimens. These thicker α laths became predominant in the HT875 samples (Fig. 3d). In this condition, the β layer thickness grew significantly. Moreover, a further loss of microstructural order with respect to the samples held at lower temperatures confirms the previous hypothesis on the disappearance of clear colonies. Furthermore, in correspondence of the largest β-rich areas, a very fine α sub-structure was found. It was formed by very fine α laths (approximately 100 nm mean width) in a β matrix. The α phase was then present both as primary and secondary α, at decreasing sizes respectively. Hence, the overall microstructure can be defined as hierarchical, due to the presence of diverse structures at different levels of scale. In titanium metallurgy, such microstructures are often labelled as bi-lamellar [31]. These are associated with an improvement in most mechanical properties, in particular YTS and ε, due to a decrease in slip length, with respect to a purely lamellar microstructure [32]. In fact, slip can transfer from α to β phase, even if they deform independently and their relative interface is incoherent. This phenomenon occurs due to the presence of two slip systems of the HCP and BCC crystals that are parallel/quasi-parallel. As a consequence of that, in a lamellar microstructure the slip length equals the colony size. In
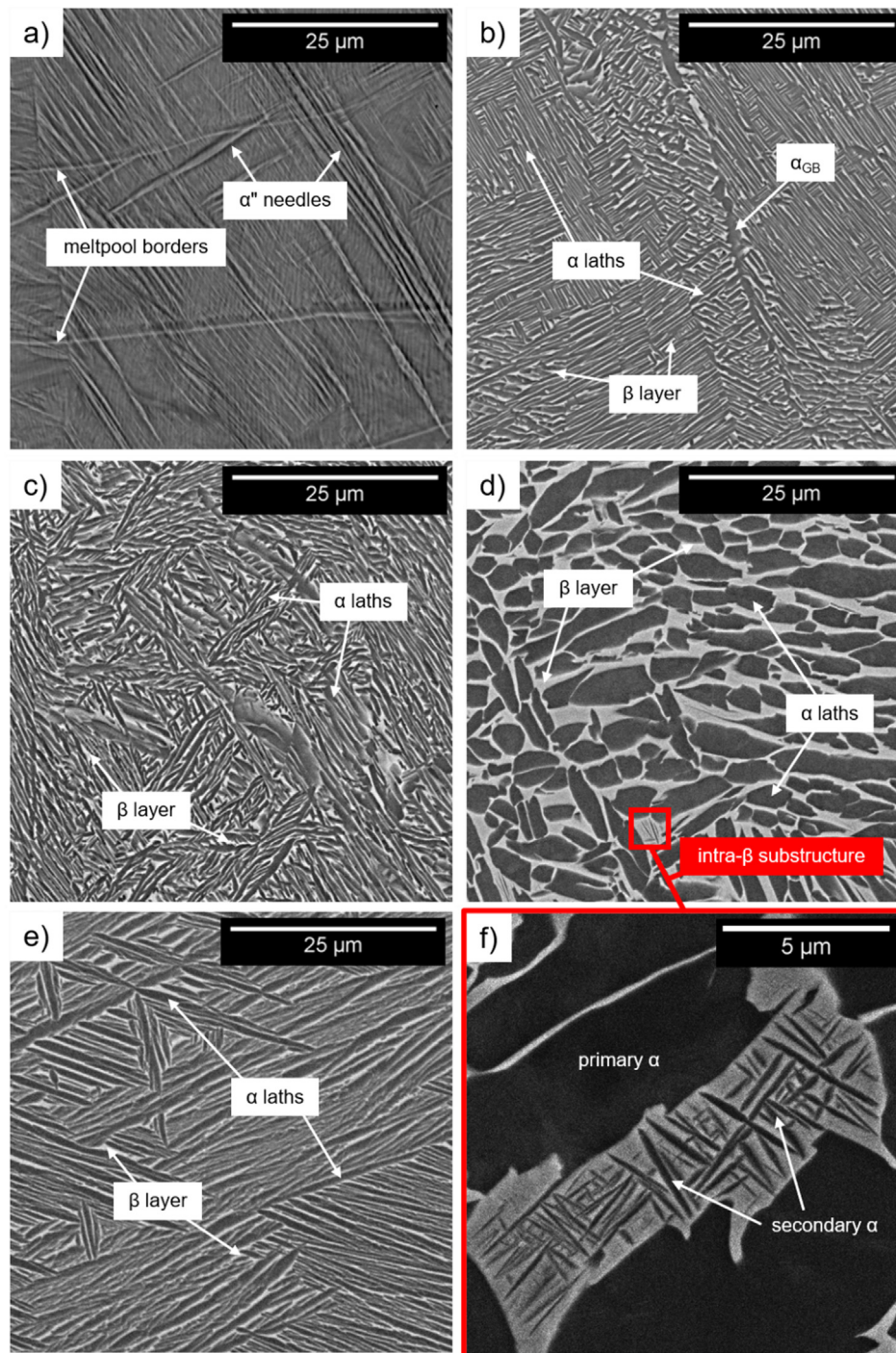
Fig. 3. SEM micrographs of the as-built (a), HT600 (b), HT750 (c), HT875 (d) and HT950 (e) conditions. Higher-magnification image of a hierarchical intra-β substructure found in the HT875 sample (f).

a bi-lamellar microstructure instead, the softer β phase is hardened by the fine α platelets, thus reducing the effective slip length to the size of a single α lath [31,32]. Generally, in order to obtain this type of microstructures in conventional α + β titanium alloys (e.g. Ti-6Al-4 V), a complex post-processing route is usually needed, characterized by multi-steps heat treatments [32,33]. In this case, the achievement of such sub-structure via a simple annealing treatment might be the result of the Ti-6Al-2Sn-4Zr-6Mo alloy being highly β-stabilized, thus providing high-volume β regions, acting as preferential nucleation spots for new α laths. Finally, the HT950 samples provided a shift from a columnar prior-β grains

morphology, commonly shared by all the other specimens, to an equiaxed morphology, due to the recrystallisation of the microstructure, caused by the isothermal hold being conducted at T > T_β. An α + β microstructure was detected, in which the α lamellae appeared both grouped in colonies and arranged in a Widmanstätten pattern, recognizable by the typical ± 30/60° between neighbour lamellae. The coexistence of both structures proved that the cooling rate achieved at the end of the heat treatment was intermediate. In fact, a Widmanstätten morphology is usually achieved at higher cooling rates than a lamellar microstructure [32,34].
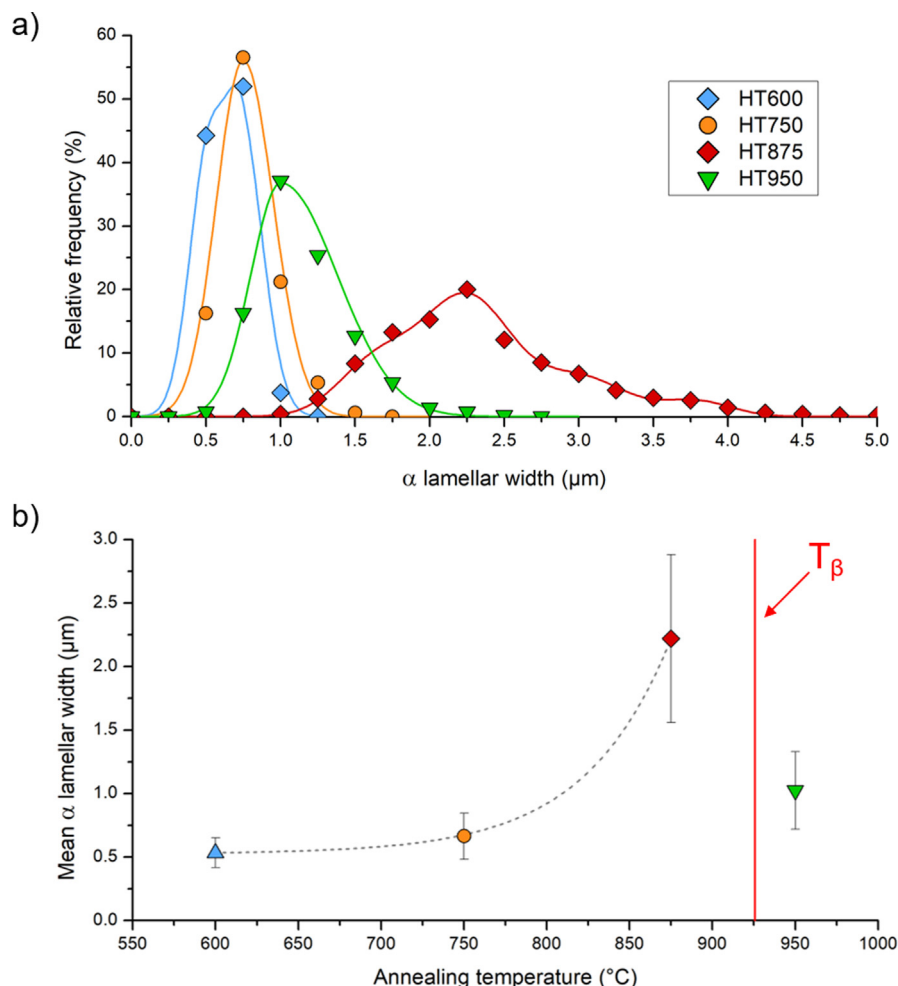
Fig. 4. α width distributions (a) and relative mean values (b) for the heat-treated specimens.

The width of the α laths was chosen as the microstructural parameter best-suited to numerically compare the microstructures investigated (Fig. 4). This step is important due to the direct correlation between the size of the α lamellae and the mechanical properties of the material [28,32]. For example, Han et al. [35] reported decreasing strength and increasing elongation values for a lamellar microstructures that experiences growth phenomena. In general, the specimens annealed at T < $T_β$ provided distribution curves shifted towards higher α width values for increasing treatment temperatures. This trend is related to the diffusional nature of the β → α + β transformation that occurs upon cooling. Moreover, the time required by the system to reach room temperature increases if the furnace must cool down from higher temperatures, thus further favouring α growth. In fact, the mean width values for the samples in the HT600 (0.53 μm), HT750 (0.66 μm) and HT875 (2.22 μm) conditions resulted in a quasi-parabolic distribution at increasing isothermal holding temperatures (Fig. 4b). When the heat treatment was conducted at T > $T_β$ instead (HT950), the resulting microstructure was characterized by significantly thinner lamellae (1.02 μm on average) with respect to the specimens in the HT875 condition, even if the isothermal holding occurred at higher temperatures. This phenomenon is the result of the 100% β content that characterized the material at high temperatures. In fact, in this case, upon cooling α phase nucleated directly from β. On the opposite, when the isothermal holding was conducted at T < $T_β$, the residual α phase experienced immediately growth

phenomena of the residual α phase from room temperature. As a result of that, the α laths were progressively characterized by a decrease in the aspect ratio, i.e. HT600 and HT875 (Fig. 3b,d), until a T > $T_β$ was reached, then the newly generated lamellae appeared again extremely elongated in the HT950 condition (Fig. 3e).

XRD analyses (Fig. 5) confirmed the phase composition assumed from the micrographs in Fig. 3. Thus, all the heat-treated specimens provided a α + β microstructures. In particular, the HT600 samples were characterized by a lack of peaks relative to the metastable martensite α". Hence, the DSC peak I in Fig. 2 can be related to the decomposition of this phase and the 567–686 °C range can be associated to the temperature range in which the martensitic decomposition occurs, for this specific heating conditions. Since peaks I and II in the DSC analyses were associated to the α" → α + β transformation and stress relaxation phenomena, the latter phenomenon might take place higher temperatures (Peak II). This assumption seemed to be confirmed by the shift of XRD peaks (e.g. Ti-α (1 0 1) peak in Fig. 5b) of the specimens in the HT600 condition, with respect to the other heat-treated samples. This alteration might be attributed to the persistence of the residual stresses, caused by the manufacturing process, in the HT600 condition [36]. In fact, the evaluation of the cell volume from the XRD patterns resulted in a significant contraction of the α and β lattices in the HT600 state (Fig. 5c), with respect to the other specimens, which provided similar values instead [37]. This last information seems to confirm that stress relieving occurs at
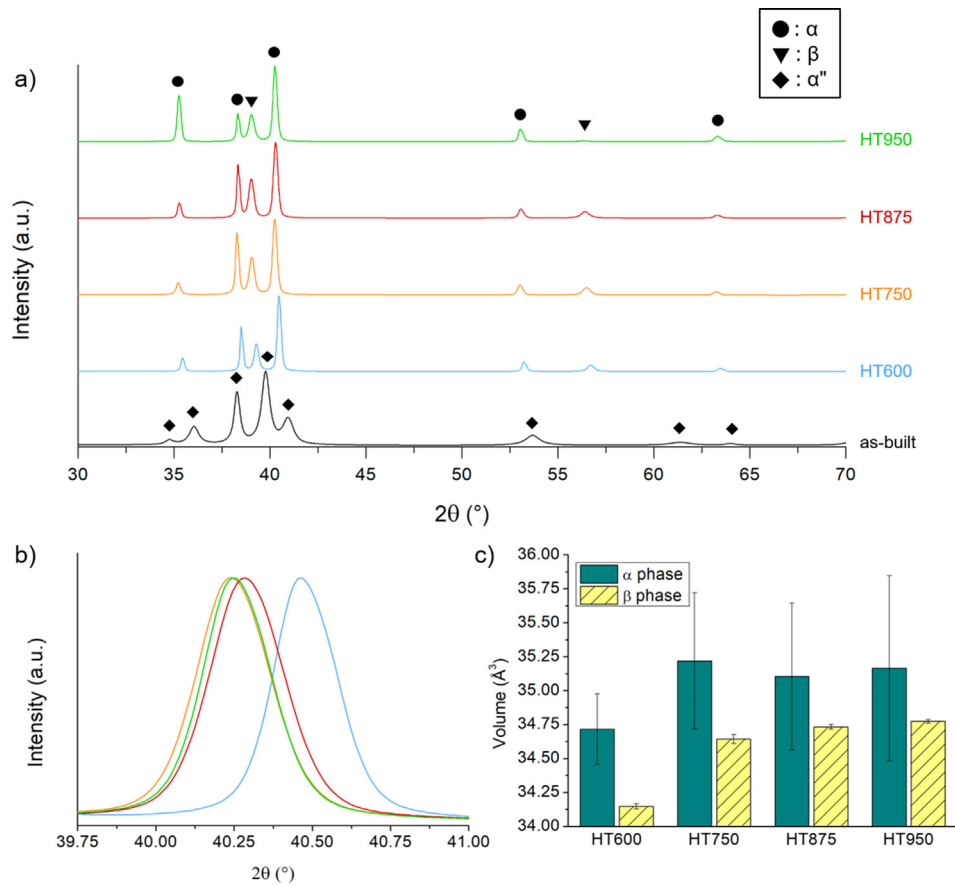
Fig. 5. XRD spectra of the as-built and heat-treated specimens (a) with a comparison of the Ti-α (1 0 1) peaks of all the heat-treated samples (b). Cell volume values determined for the heat-treated specimens (c).

T greater than 750 °C. However, since this type of transformation is both time and temperature dependant, a second DSC analysis was conducted in order to check whether stress-relieving still occurred in the specimens in the HT600 conditions. The relative thermogram, provided in Fig. 6, confirmed that peak II was unaffected by an isothermal holding at 600 °C, hence its activation energy is high enough to require higher temperatures in order to activate. Hence, the DSC peak II in Fig. 2 can be effectively attributed to stress relaxation, which then occurs approximately in the 686–855 °C range, for the heating conditions used in this work.

The exothermic transformations (martensite decomposition and stress relaxation) occurring during the heating phase in the Ti-6Al-2Sn-4Zr-6Mo alloy are coherent with the ones presented by Sallica-Leva et al. [18] in the LPBF-produced Ti-6Al-4 V alloy. The different temperature ranges for both transformations between these two works can be attributed to the different types of martensite involved (α' and α") and the different compositions of the materials considered. However, the two alloys in exam also differ in terms of the order in which the transformations take place. In fact, in the Ti-6Al-4 V alloy, stress relieving occurs before martensite decomposition [18]. On the contrary, in the Ti-6Al-2Sn-4Zr-6Mo the opposite phenomenon takes place. Therefore, even if the α" → α + β decomposition generates a change from an orthorhombic to hcp and bcc lattices, the crystallographic strain due to the residual stresses, generated by the LPBF process, is still retained.

The mean Vickers microhardness was measured in all the samples, providing the results reported in Fig. 7a. The lowest microhardness values were measured in the specimens in the as-built

and HT875 states, both characterized by mean values of 339 HV. The low performance of the as-built samples might be attributed to the presence of the soft α" martensite [38]. In contrast, the specimens in the HT875 condition experienced a drop in hardness probably due to the very coarse α microstructure. Overall, a good inverse linear correlation between α width and hardness ($R^2 = 0.94$) was found when comparing all the heat-treated samples (Fig. 7b). Hence, a drop in the hardness value can be expected for a rougher lamellar microstructure, as confirmed by similar results in the literature obtained for the Ti-6Al-4 V alloy [39].

The main tensile properties are summarized in Fig. 8. As illustrated in a previous work [12], the as-printed specimens provided a significantly low mean YTS value (483 ± 6 MPa) and outstanding ε (25 ± 2%). This unique combination of mechanical properties is the result of the massive presence of the orthorhombic martensite, which has a strong detrimental effect on strength coupled with a significant softening character. Since all the specimens in the other conditions did not provide any trace of α", a substantial augment in strength occurred after all the heat treatments were conducted. The specimens in the HT600 condition provided outstanding YTS (1383 ± 8 MPa) and UTS (1457 ± 18 MPa). The authors attributed these impressive values to the extensive lattice strain experienced by the specimens in this condition, as confirmed by the XRD data (Fig. 5b,c), coupled with the absence of a", which caused significant softening in the as-built state. The contraction of the lattice due to the residual stresses, induced by the unique solidification path that the material underwent during LPBF processing, might have affected the tensile behaviour of the alloy extensively [40]. In general, lattice distortions cause a certain amount of elastic energy to
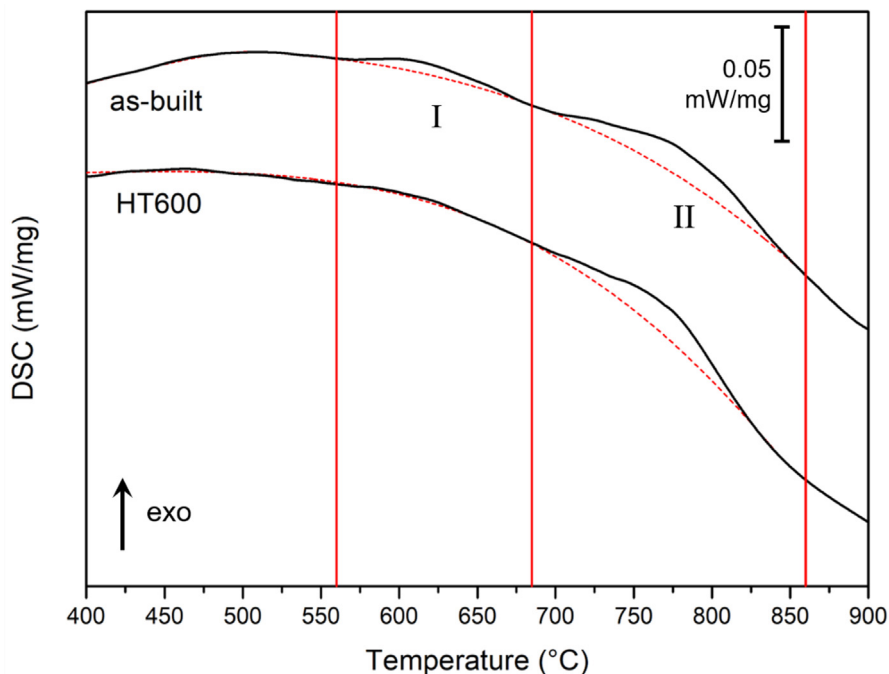
Fig. 6. Comparison of the DSC thermograms of two samples in the as-built and HT600 state, focusing on peak I and II, identified by the previous analysis. The dashed red line (baseline) highlights the exothermic peaks. (For interpretation of the references to colour in this figure legend, the reader is referred to the web version of this article.)
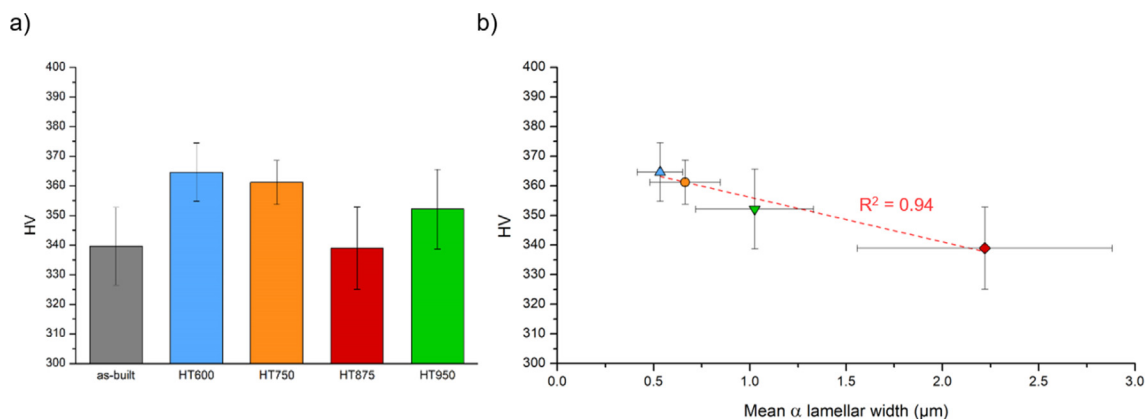

Fig. 7. Average Vickers microhardness values evaluated for all the conditions considered in this work (a) and hardness-lamellar width trend of the heat-treated specimens (b).
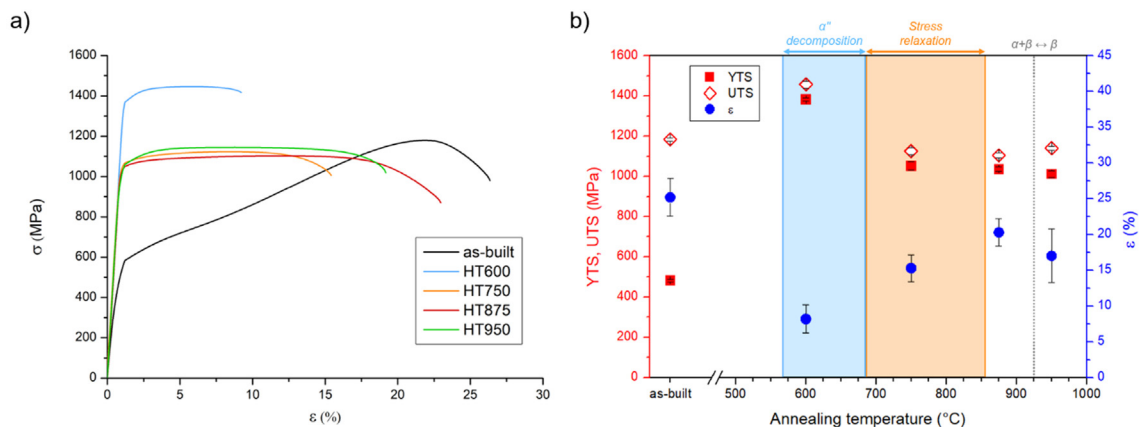

Fig. 8. Stress-strain curves of the as-built and heat-treated LPBF-produced Ti-6Al-2Sn-4Zr-6Mo specimens (a) and relative average YTS, UTS and ε (b).

be stored. This effect results in hindering of the motion of the dislocations, thus isotropic hardening of the alloy [41,42]. In fact, a reduced dislocation mobility might result in the material being able to withstand higher loads before plastically deforming during the tensile test, in accordance with our data. The resulting ductility is certainly decreased as a consequence of that [43]. To sum up, the overall effect that took place was similar to solid solution strengthening, which cause a variation in the lattice size/shape, thus causing strengthening and reduced ductility, due to a decrease in dislocation mobility.

The HT750, HT875 and HT950 samples were characterized by similar YTS and UTS values, ranging from 1000 to 1050 MPa and 1125 to 1140 MPa, respectively. This behaviour is expected to be the result of phase composition shifting from α" to α + β. A continuous ductility improvement at progressively higher temperatures for T < T_β was also detected. This phenomenon was probably correlated to the size of the α laths (Fig. 4). Thus, the samples in the HT875 condition proved to be the most performing in terms of ductility. This behaviour was probably caused by the hierarchical α + β microstructure, which granted a reduced slip length. Usually, a decrease in slip length causes a simultaneous increase in ductility and strength. However, in this case the latter phenomenon was probably counterbalanced by the overall microstructural coarsening taking place at high temperatures (Fig. 4). Instead, the HT750 and HT950 samples provided similar tensile properties, even if different microstructural features/morphologies were achieved. The comparable YTS, UTS and ε value were the result of distinct strengthening mechanisms, related to, for example, finer prior-β grains or α laths. Furthermore, it is also important to underline that the heat-treating at 950 °C implies the shift from a columnar to an equiaxed grain morphology, which results in an improvement in terms of isotropy in the HT950 specimens.

To further assess the mechanical behaviour of the samples, the fracture surfaces resulted from the tensile tests were investigated, as visible in Fig. 9. The as-built specimens (Fig. 9a) were characterized by a massive presence of large dimples throughout the whole surface, suggesting a completely ductile behaviour, thus confirming the outcome of the tensile test. The specimens in the HT750, HT875 and HT950 conditions (Fig. 9c,d,e) provided a mixed brittle-ductile fracture mode instead. In fact, quasi-cleavage facets and dimples appeared alongside each other on the surface. Conversely, the samples in the HT600 state (Fig. 9b) provided a significantly brittler fracture surface, characterized by a very limited number of dimples visible. In contrast, the quasi-cleavage surfaces (tear ridges) were predominant, thus confirming the significantly lower ductility recorder during the tensile tests.

4. Conclusions

In this work, the phenomena taking place in the LPBF-produced Ti-6Al-2Sn-4Zr-6Mo alloy during different heat treatments were studied. The aim of this evaluation was to generate a deep understanding of how these transformations affect the mechanical properties. These data are fundamental to tailor the properties of the material according to the requirements dictated by the final application.

The main results can be summarised as follows:.

- In the as-built state, the microstructure of the Ti-6Al-2Sn-4Zr-6Mo alloy is characterized by α" orthorhombic martensite, which Provides low strength (≈ 500 MPa), outstanding ductility (≈ 25%) and quite low hardness (340 HV).
- At 600 °C the α" → α + β transformation takes place, thus resulting in a significant increase in strength (1383 MPa), associated with a severe ε reduction (8.2 %) and an augment in terms of hardness (365 HV). The residual stress was retained.
- At 750 °C residual stress relaxation occurred, thus softening the material (YTS = 1052 MPa) and greatly improving its ductility (15.3%). Hardness was unaffected by the stress relaxation (361 HV).
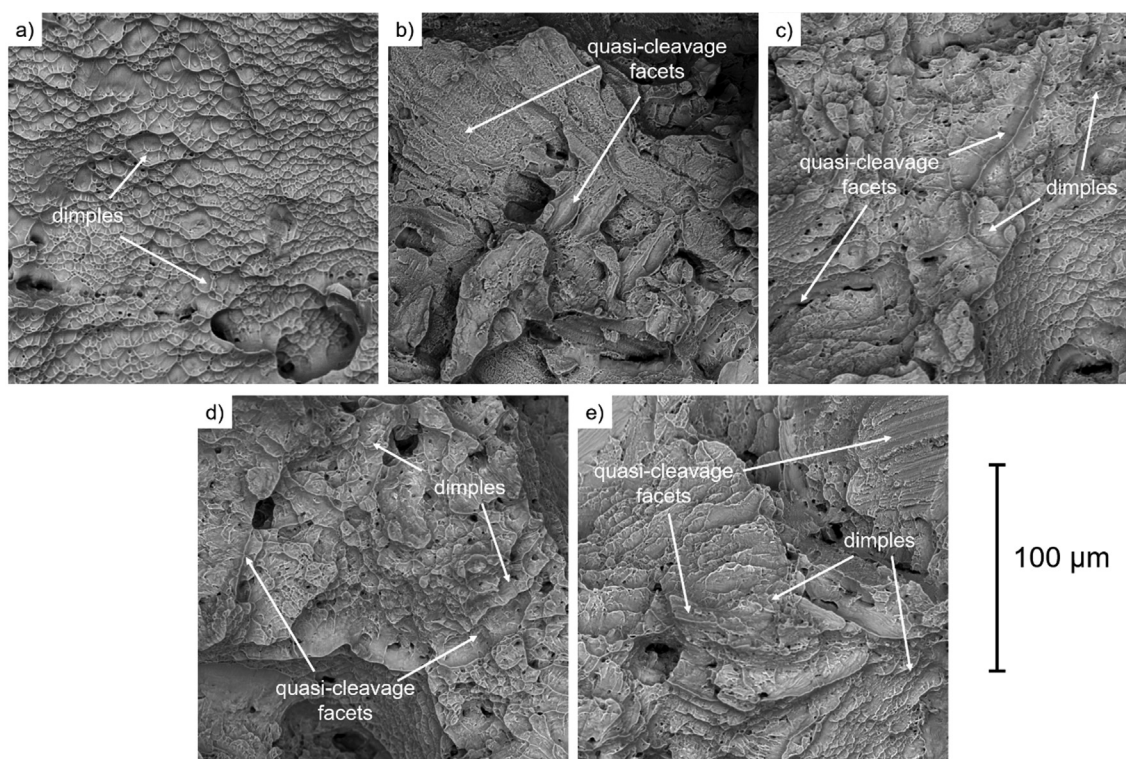

Fig. 9. Fracture surfaces of the tensile samples in the as-built (a), HT600 (b), HT750 (c), HT 875 (d) and HT950 (e) states.

- At 875 °C, a bi-lamellar microstructure was observed. This led to a further improvement of the ductility (20.3%), retaining an optimal strength value (1037 MPa). A significant drop in hardness was detected (339 HV), probably due to extensive microstructural coarsening.
- At 950 °C (T > T$_\beta$), a small drop in strength (1012 MPa) and ductility (17%) were measured. Conversely, hardness increased (352 HV). However, since a complete recrystallization of the microstructure occurred, isotropy was improved by getting rid of the columnar prior-β grains.

Declaration of Competing Interest

The authors declare that they have no known competing financial interests or personal relationships that could have appeared to influence the work reported in this paper.

Acknowledgements

Funding

References

[1] M. Whittaker, Titanium in the gas turbine engine, in: Adv. Gas Turbine Technol., BoD–Books on Demand, 2011.

[2] R. Pederson, The microstructures of Ti-6Al-4V and Ti-6Al-2Sn-4Zr-6Mo and their relationship to processing and properties, 2004. doi:ISSN 1402-1544 / ISRN LTU-DT–04/19–SE / NR 2004:19.

[3] R. Pederson, F. Niklasson, F. Skystedt, R. Warren, Microstructure and mechanical properties of friction-and electron-beam welded Ti–6Al–4V and Ti–6Al–2Sn–4Zr–6Mo, Mater. Sci. Eng. A. 552 (2012) 555–565.

[4] B. Dutta, F.H. Froes, The Additive Manufacturing (AM) of titanium alloys, in: Elsevier (Ed.), Titan. Powder Metall., 2015: pp. 447–468.

[5] F. Trevisan, F. Calignano, A. Aversa, G. Marchese, M. Lombardi, S. Biamino, D. Ugues, D. Manfredi, Additive manufacturing of titanium alloys in the biomedical field: processes, properties and applications, J. Appl. Biomater. Funct. Mater. 16 (2) (2018) 57–67, https://doi.org/10.5301/jabfm.5000371.

[6] S.E. Brika, M. Letenneur, C.A. Dion, V. Brailovski, Influence of particle morphology and size distribution on the powder flowability and laser powder bed fusion manufacturability of Ti-6Al-4V alloy, Addit. Manuf. 31 (2020) 100929.

[7] Y. Xiao, N. Dai, Y. Chen, J. Zhang, S.-W. Choi, On the microstructure and corrosion behaviors of selective laser melted CP-Ti and Ti-6Al-4V alloy in Hank's artificial body fluid, Mater. Res. Express. 6 (2019) 126521.

[8] L.C. Zhang, D. Klemm, J. Eckert, Y.L. Hao, T.B. Sercombe, Manufacture by selective laser melting and mechanical behavior of a biomedical Ti–24Nb–4Zr–8Sn alloy, Scr. Mater. 65 (1) (2011) 21–24.

[9] T. Marcu, M. Todea, I. Gligor, P. Berce, C. Popa, Effect of surface conditioning on the flowability of Ti6Al7Nb powder for selective laser melting applications, Appl. Surf. Sci. 258 (7) (2012) 3276–3282.

[10] M. Speirs, J.V. Humbeeck, J. Schrooten, J. Luyten, J.P. Kruth, The effect of pore geometry on the mechanical properties of selective laser melted Ti-13Nb-13Zr scaffolds, Procedia Cirp. 5 (2013) 79–82.

[11] L. Zhou, T. Yuan, R. Li, J. Tang, M. Wang, F. Mei, Microstructure and mechanical properties of selective laser melted biomaterial Ti-13Nb-13Zr compared to hot-forging, Mater. Sci. Eng. A. 725 (2018) 329–340, https://doi.org/10.1016/j.msea.2018.04.001.

[12] A. Carrozza, A. Aversa, P. Fino, M. Lombardi, A study on the microstructure and mechanical properties of the Ti-6Al-2Sn-4Zr-6Mo alloy produced via Laser Powder Bed Fusion, J. Alloys Compd. 870 (2021) 159329, https://doi.org/10.1016/j.jallcom.2021.159329.

[13] H. Hassanin, Y. Zweiri, L. Finet, K. Essa, C. Qiu, M. Attallah, Laser powder bed fusion of Ti-6Al-2Sn-4Zr-6Mo alloy and properties prediction using deep learning approaches, Materials (Basel). 14 (2021) 2056.

[14] Z. Zou, M. Simonelli, J. Katrib, G. Dimitrakis, R. Hague, Microstructure and tensile properties of additive manufactured Ti-6Al-4V with refined prior-β grain structure obtained by rapid heat treatment, Mater. Sci. Eng. A. 814 (2021) 141271, https://doi.org/10.1016/j.msea.2021.141271.

[15] M. Carton, P. Jacques, N. Clément, J. Lecomte-Beckers, Study of transformations and microstructural modifications in Ti-LCB and Ti-555 alloys using differential scanning calorimetry, Ti-2007, Sci. Technol. (2007) 491–494.

[16] K. Yildiz, M. Kok, Study of martensite transformation and microstructural evolution of Cu–Al–Ni–Fe shape memory alloys, J. Therm. Anal. Calorim. 115 (2) (2014) 1509–1514.

[17] K. Kus, T. Breczko, DSC-investigations of the effect of annealing temperature on the phase transformation behaviour in Ni-Ti shape memory alloy, Mater. Phys. Mech. 9 (2010) 75–83.

[18] E. Sallica-Leva, R. Caram, A.L. Jardini, J.B. Fogagnolo, Ductility improvement due to martensite α' decomposition in porous Ti-6Al-4V parts produced by selective laser melting for orthopedic implants, J. Mech. Behav. Biomed. Mater. 54 (2016) 149–158, https://doi.org/10.1016/j.jmbbm.2015.09.020.

[19] Z. Liang, Z. Sun, W. Zhang, S. Wu, H. Chang, The effect of heat treatment on microstructure evolution and tensile properties of selective laser melted Ti6Al4V alloy, J. Alloys Compd. 782 (2019) 1041–1048.

[20] W.M.I. Makhetha, T.H. Becker, N. Sacks, Post-Processing Framework for As-Built LPBF Ti-6Al-4V Parts Towards Meeting Industry Functional Requirements, JOM. 74 (3) (2022) 764–776.

[21] M. Young, E. Levine, H. Margolin, Aging Behavior of Orthorhombic Martensite in Ti-6-2-4-6, Met. Trans. 5 (1974) 1891–1898, https://doi.org/10.1007/BF02644157.

[22] P. Stella, I. Giovanetti, G. Masi, M. Leoni, A. Molinari, Microstructure and microhardness of heat-treated Ti-6Al-2Sn-4Zr-6Mo alloy, J. Alloys Compd. 567 (2013) 134–140, https://doi.org/10.1016/j.jallcom.2013.03.046.

[23] M.S. Hussain, C. Siemers, J. Rösler, Development of a free-machining (α+ β) titanium alloy based on Ti-6Al-2Sn-4Zr-6Mo, Mater. Manuf. Process. 28 (2013) 545–549.

[24] A. Carrozza, A. Aversa, F. Mazzucato, M. Lombardi, S. Biamino, A. Valente, P. Fino, An Innovative Approach on Directed Energy Deposition Optimization : A Study of the Process Environment's Influence on the Quality of Ti-6Al-4V Samples, Appl. Sci. 10 (2020).

[25] E. Astm, Standard test methods for tension testing of metallic materials, Annu. B. ASTM Stand, ASTM, 2001.

[26] D. V. Gadeev, A.G. Illarionov, Determination of beta-transus temperature of two-phase titanium alloys using differential scanning calorimetry, Solid State Phenom. 284 SSP (2018) 259–264. doi:10.4028/www.scientific.net/SSP.284.259.

[27] P. Fima, A. Gazda, Thermal analysis of selected Sn–Ag–Cu alloys, J. Therm. Anal. Calorim. 112 (2) (2013) 731–737.

[28] M.J. Donachie, Titanium: a technical guide, ASM international (2000).

[29] H. Shipley, D. McDonnell, M. Culleton, R. Coull, R. Lupoi, G. O'Donnell, D. Trimble, Optimisation of process parameters to address fundamental challenges during selective laser melting of Ti-6Al-4V: A review, Int. J. Mach. Tools Manuf. 128 (2018) 1–20, https://doi.org/10.1016/j.ijmachtools.2018.01.003.

[30] J.C. Chesnutt, C.G. Rhodes, J.C. Williams, Relationship between mechanical properties, microstructure, and fracture topography in α+ β titanium alloys, in: Fractography—Microscopic Crack. Process., ASTM International, 1976.

[31] G. Lütjering, Influence of processing on microstructure and mechanical properties of (α+ β) titanium alloys, Mater. Sci. Eng. A. 243 (1-2) (1998) 32–45.

[32] G. Lütjering, J.C. Williams, Titanium Book (2007), https://doi.org/10.10007/978-3-540-71398-2.

[33] Y. Chong, T. Bhattacharjee, N. Tsuji, Bi-lamellar microstructure in Ti–6Al–4V: Microstructure evolution and mechanical properties, Mater. Sci. Eng. A. 762 (2019) 138077, https://doi.org/10.1016/j.msea.2019.138077.

[34] C. Leyens, M. Peters, Titanium and titanium alloys: fundamentals and applications, 2003.

[35] Y. Han, F. Zhao, Y. Liu, C. Huang, Quantitative Relationships between Mechanical Properties and Microstructure of Ti17 Alloy after Thermomechanical Treatment, Metals (Basel). 10 (2020) 67.

[36] B.D. Cullity, S.R. Stock, Elements of X-Ray Diffraction, Addison-Wesley Publishing (1956).

[37] J.-S. Park, A.K. Ray, P.R. Dawson, U. Lienert, M.P. Miller, Determination of residual stress in a microtextured α titanium component using high-energy synchrotron X-rays, J. Strain Anal. Eng. Des. 51 (5) (2016) 358–374.

[38] Y. Guo, T. Jung, Y.L. Chiu, H. Li, S. Bray, P. Bowen, Microstructure and microhardness of Ti6246 linear friction weld, Mater. Sci. Eng. A. 562 (2013) 17–24, https://doi.org/10.1016/j.msea.2012.10.089.

[39] J.S. Zuback, T. DebRoy, The hardness of additively manufactured alloys, Materials (Basel). 11 (12) (2018) 2070, https://doi.org/10.3390/ma11112070.

[40] T. Maimaitiyili, R. Woracek, M. Neikter, M. Boin, R. Wimpory, R. Pederson, M. Strobl, M. Drakopoulos, N. Schäfer, C. Bjerkén, Residual lattice strain and phase distribution in Ti-6Al-4V produced by electron beam melting, Materials (Basel). 12 (4) (2019) 667, https://doi.org/10.3390/ma12040667.

[41] B. Babu, Physically based model for plasticity and creep of Ti-6Al-4V, Luleå tekniska universitet (2008).

[42] X. Ye, Z.T.H. Tse, G. Tang, Mechanical properties and tensile fracture of Ti–Al–V alloy strip under electropulsing-induced phase change, J. Mater. Res. 30 (2) (2015) 206–223.

[43] D. Zhang, L. Wang, H. Zhang, A. Maldar, G. Zhu, W. Chen, J.-S. Park, J. Wang, X. Zeng, Effect of heat treatment on the tensile behavior of selective laser melted Ti-6Al-4V by in situ X-ray characterization, Acta Mater. 189 (2020) 93–104.